BMC Plant Biology

RESEARCH

Open Access

Integrated omic analysis provides insights into how *Cuscuta australis* inhibits the growth and reproduction of *Xanthium spinosum*

Yunxia Wang[1†], Hubai Bu[1†], Xin Gu[2], Wanxue Liu[3] and Xinpu Wang[2*]

Abstract

Background *Xanthium spinosum* is one of the most abundant and aggressively invasive plants in the world. *Cuscuta australis* parasitism hinders *X. spinosum* growth and development by absorbing nutrients, leading to reduced reproductive performance. However, which metabolite changes contribute to stunted growth and diminished reproductive performance in *X. spinosum*? Additionally, what genes regulate these metabolites? These underlying mechanisms remain largely unknown.

Results *X. spinosum* was used to determine the physiological relevance of *C. australis* parasitism to alleviate host plant growth and explore the molecular mechanism, with a focus on metabolic pathways. The results revealed that *C. australis* significantly reduced the growth potential of *X. spinosum*, with a particularly notable decrease in seed quantity, which decreased by 92.07%. *C. australis* parasitism increased the activities of the peroxidase (POD) and superoxide dismutase (SOD) enzymes in the stems of *X. spinosum*. Integrated transcriptome and metabolome analysis revealed that *C. australis* influenced lignin synthesis in the stem through the phenylpropanoid biosynthesis pathway. Concurrently, the majority of differentially expressed genes in the galactose metabolism pathway were upregulated, leading to increased sugar accumulation and disrupted metabolism. Furthermore, all differentially expressed genes in the autophagy-other pathway were upregulated, resulting in excessive autophagy and a significant reduction in the reproductive performance of *X. spinosum*.

Conclusions The results provide a theoretical foundation for the development of targeted pesticides aimed at controlling *X. spinosum*.

Keywords *Xanthium spinosum*, *Cuscuta australis*, Growth and development, Reproductive performance, Metabolic pathways

Background

Invasive alien species (IASs) have been brought by humans to areas outside their native ranges, representing one of the primary direct causes of biodiversity decline [1, 2]; these organisms are increasingly viewed as a developing global health challenge, altering the socioecological environment where billions reside, diminishing natural resilience to various disturbances, and transforming local ecological dynamics [3–5]. In particular, China is among the countries most severely affected by IASs stress and has the weakest ability to defend against IASs

†Yunxia Wang and Hubai Bu contributed equally to this work

*Correspondence:
Xinpu Wang
wangxinpu@nxu.edu.cn
[1] College of Forestry and Prataculture, Ningxia University, Yinchuan 750021, China
[2] Agricultural College of Ningxia University, Yinchuan 750021, China
[3] State Key Laboratory for Biology of Plant Diseases and Insect Pests, Institute of Plant Protection, Chinese Academy of Agricultural Science, Beijing 100193, China

[6]. The natural disaster caused by IASs has resulted in direct economic losses of approximately 7623.85 billion yuan in China [7].

Xanthium spinosum Linn. (Compositae) is a poisonous invasive summer annual weed native to Argentina; it is distributed worldwide but is most widely distributed in Central and Southern Europe and the Pacific Northwest [8–10]. It has been listed as one of the worst invasive alien species in China. *X. spinosum* was first discovered in 1932 in Dancheng County, Henan Province, China, and is now widely distributed in Anhui, Beijing, Ningxia and other provinces in China [9, 11]. The Ningxia Hui Autonomous Region is located in inland Northwest China; its ecosystem structure is relatively simple and fragile, making it particularly susceptible to the negative impacts of IASs. The barbed surface of the involucre of *X. spinosum* facilitates its unintentional spread by humans and transfer via the fur of animals, enabling it to rapidly invade large areas [12, 13]. Therefore, sheep grazing in Ningxia, China, is particularly troublesome. *X. spinosum* has invaded farmland along roads and surrounding villages in desert areas and has caused severe damage to ecosystems and local economies. Therefore, the prevention and control of *X. spinosum* is an urgent challenge. Research in this field has focused mainly on the separation and identification of *X. spinosum* active components, secondary metabolite allelopathy, invasion and distribution, and interspecific competition [14–17]. However, there are few reports on the control of *X. spinosum*. Chemical control is temporarily effective but often causes environmental pollution. Biological control methods are particularly appealing because of their environmentally friendly characteristics [10]. Research has indicated that a naturally occurring fungal pathogen of *X. spinosum*, *Colletotrichum orbiculare* [18], does not seem to have diminished the abundance of the weed. Additionally, most insects that attack these introduced weeds are polyphagous, sap-feeding or foliage-feeding species, and they do not seem to exhibit an obvious control effect [19].

Cuscuta australis is a member of the Convolvulaceae family and is classified as a parasitic angiosperm. *C. australis* attaches to the vascular tissue of a host plant via haustoria to facilitate nutrient absorption. *Cuscuta* species significantly inhibit the reproductive capacity of host plants, offering a potential eco-friendly alternative that can be used as a control method [20]. Studies have shown that *Cuscuta* parasitism hinders growth and development by absorbing nutrients from *Mikania* [20] and *Bidens pilosa* [21], leading to their decline. Only one study has examined the effects of *Cuscuta* parasitism on the growth and development of *Xanthium* weeds from a physiological standpoint (in Chinese). However, what specific material changes result in a significant decrease in the reproductive performance of these invasive plants? Additionally, which genes regulate these substances? These mechanisms remain unclear. Moreover, the widespread distribution of *Cuscuta* presents serious environmental hazards, making its direct application for the prevention and control of invasive plants challenging. In this study, *X. spinosum* was parasitized with *C. australis,* with the aim of characterizing the metabolic and transcriptional alterations observed in the parasitized stems of *X. spinosum*. Elucidating the possible target of action by which *Cuscuta* inhibits the growth and reproduction of *X. spinosum* is crucial for understanding the mechanisms through which dodder inhibits the growth of invasive plants, laying a theoretical foundation for the development of scientific and ethical alternatives. The results of this study reveal the systemic impact of *C. australis* parasitism on the gene regulatory network of *X. spinosum*, identify specific markers of the parasitic effects of *C. australis*, and fill the knowledge gap in the development of targeted pesticides against *X. spinosum*.

Materials and methods

Plant materials and environmental conditions

This study was restricted to Yinchuan city, the capital of the Ningxia Hui Autonomous Region, which is situated in northwestern China. The sample plots were located on Machang Road, Xixia district, China. The climate in the area is continental, with average rainfall ranging from 180–210 mm and evaporation ranging from 1100–1650 mm [22]. The plot was composed of coexisting communities of *X. spinosum*, *C. australis*, *Chloris virgata*, *Chenopodium album* and other plants. These plants were identified by Lei Zhang, North University for Nationalities, China. A *X. spinosum* (zlnmu2022189) specimen was uploaded to the National Plant Specimen Resource Center (NPSRC) (https://www.cvh.ac.cn/spms/detail.php?id=b1c86057). *X. spinosum* plants were divided into plots infested and noninfested (control) with *C. australis* on July 01, 2023. For each treatment, three replicate plots (20 × 30 m) were established. To prevent cross-contamination, plots were monitored every 5 days to ensure that *C. australis* did not spread from infested areas to noninfested areas. At peak fruiting (September 05, 2023), plants were sampled using a 5-point sampling method (4 plants per point, totaling 20 plants per plot) to measure the plant height, stem thickness, leaf number, leaf area and seed quantity of both parasitized and unparasitized plants. From each sampling point, stems of three randomly selected *X. spinosum* plants were collected immediately following *C. australis* removal. The samples were flash-frozen in liquid nitrogen, with three biological replicates per treatment group. These samples

were subsequently used for antioxidative enzyme activity assays, metabolomic profiling and transcriptome sequencing.

Analyses of antioxidant enzyme activities

Antioxidant enzyme activities were determined in parasitized and unparasitized stems. The extraction and analysis processes were performed in accordance with the instructions provided in a kit. The levels of antioxidant enzymes, including superoxide dismutase (SOD), peroxidase (POD), and catalase (CAT), were determined using test kits (A001-3–2, A084-3–1, and A007-1–1) obtained from Nanjing Jiancheng Bioengineering Institute (Nanjing, China). SOD activity was determined using the 4-[3-(4-iodophenyl)−2-(4-nitrophenyl)−2 H-5-tetrazolio]−1,3-benzene disulfonate (WST-1) method; POD activity was measured using the guaiacol method; and CAT activity was determined using the ammonium molybdate method [23]. Relevant kit manuals were used for the preparation of reagents I, II, III and IV and specific operations.

Untargeted metabolic analysis

Metabolite extraction and metabolite measurements were carried out by OE Biotechnology Co., Ltd. (Shanghai, China), with six biological replicates. For metabolite extraction, a total of 60 mg of sample was introduced into a 1.5 mL Eppendorf tube, which contained 600 μL of L-2-chlorophenylalanine dissolved in methanol (0.06 $mg{\cdot}mL^{-1}$), serving as the internal standard. To ensure thorough mixing of the sample and the internal standard, two small steel balls were added to the tube, and the tube was vortexed for 10 s. After 2 min of precooling in the refrigerator at −40 °C, the sample was ground in a frozen tissue grinder (60 Hz, 2 min). The sample was subsequently sonicated in an ice–water bath using a sonicator for 30 min, after which the sample was left overnight at −40 °C. The extract was centrifuged at a speed of 13,000 revolutions per minute (rpm) for 10 min at a temperature of 4 °C. The supernatant (150 μL) was collected from each tube and filtered through microfilters with a pore size of 0.22 μm. The filtered supernatants were then transferred into high-performance liquid chromatography (HPLC) vials for subsequent analysis. Additionally, a quality control (QC) sample was created by taking 10 μL from each sample vial and combining the aliquots into a separate vial.

An ACQUITY UPLC I-Class plus (Waters Corporation, Milford, USA) coupled with a Q Exactive mass spectrometer in both ESI-positive and ESI-negative ion modes was utilized to conduct the metabolic profiling. The samples were separated with an ACQUITY UPLC HSS T3 column (1.8 μm, 2.1 × 100 mm) at constant temperature (45 °C) in both positive and negative modes. The binary gradient elution system was composed of solvent A (water with 0.1% formic acid) and solvent B (acetonitrile containing 0.1% formic acid). The following gradient was used for separation: 0.01 min, 5% B; 2 min, 5% B; 4 min, 30% B; 8 min, 50% B; 10 min, 80% B; 14 min, 100% B; 15 min, 100% B; and 15.1 min, 5% B; and 16 min, 5% B. The flow rate was 0.35 $mL{\cdot}min^{-1}$, and the injection volume was 3 μL. All the samples were stored at 4 °C throughout the analysis.

Transcriptome analysis

RNA isolation, library preparation and transcriptome sequencing were carried out by OE Biotechnology Co., Ltd. (Shanghai, China), with three biological replicates. Total RNA was extracted from the stems of parasitized and unparasitized *X. spinosum* using TRIzol in accordance with the manufacturer's instructions. RNA purity and quantity were evaluated with a NanoDrop 2000 spectrophotometer (Thermo Scientific, USA), and RNA integrity was assessed via an Agilent 2100 Bioanalyzer (Agilent Technologies, Santa Clara, CA, USA). Libraries were subsequently prepared using a VAHTS Universal V6 RNA-seq Library Prep Kit for Illumina following the manufacturer's protocol. The final step involved sequencing the libraries on the Illumina NovaSeq 6000 platform to generate 150 bp paired-end reads. There were 6 sets of original readings, including those of the invasion group (ZC-J1, ZC-J2, and ZC-J3) and the control group (N0-J1, N0-J2, and N0-J3). The raw sequence data were processed using Trimmomatic to remove poor-quality sequences and trim adaptor sequences. Trinity software (version: 2.4) was then used to assemble the clean sequencing data into transcripts for each sample. The unigenes for subsequent analysis were determined by selecting the longest transcript sequence from each gene.

The functions of the unigenes were annotated by alignment of the unigenes with the NCBI nonredundant (NR), SwissProt, and Clusters of Orthologous Groups for Eukaryotic Complete Genomes (KOG) databases via BLASTx with a threshold E value of 10^{-5}. The proteins with the highest hits to the unigenes were used to assign functional annotations. On the basis of the SwissProt annotation, Gene Ontology (GO) classification was performed by mapping the relationships between SwissProt and GO terms. The unigenes were mapped to the Kyoto Encyclopedia of Genes and Genomes (KEGG) database to annotate potential metabolic pathways.

The FPKM and read count values for each unigene were calculated using Bowtie2 and eXpress. Differentially expressed genes (DEGs) were identified using the DESeq (2012) functions estimateSizeFactors and nbinomTest. A P value < 0.05 and FC > 2 or FC < 0.5 were set as the

thresholds for significantly differential expression. Hierarchical clustering analysis of DEGs was conducted using the hclust function in R version 3.2.0. GO enrichment and KEGG pathway enrichment analyses of the DEGs were subsequently carried out using the hypergeometric distribution method.

Quantitative analysis of DEGs (RT–qPCR)

A TransScript All-in-One First-Strand cDNA Synthesis SuperMIX for qPCR kit was used to reverse transcribe the RNA samples into cDNA. A PerfectStartTM Green qPCR SuperMix Kit and a LightCycler® 480 type II fluorescence quantitative PCR instrument (Roche, Switzerland) was used to perform reactions. All procedures were conducted in accordance with the manufacturer's instructions. The gene-specific primers designed using Primer-BLAST (NCBI) are listed in Table S1. A stably expressed gene (*ARPC3*) encoding an actin-related protein was used as a reference gene for each sample. The relative expression levels of the genes were calculated using the $2^{-\Delta\Delta CT}$ method [24].

Statistical analysis

The experimental data were organized and filtered using Microsoft Excel 2021 (version 21.0). All the statistical analyses were conducted using SPSS 19.0 (SPSS Inc., Chicago, IL, USA). Morphological and physiological data were analyzed using independent-samples t tests, and normality and homogeneity of variance were analyzed using the Shapiro–Wilk test and Levene's test, respectively. A *P* value of 0.05 or less was considered statistically significant. The omics analysis involved principal component analysis (PCA), orthogonal partial least squares discriminant analysis (OPLS-DA), and a comprehensive evaluation of both the transcriptome and metabolome, all of which were conducted with R software (version 3.3.2, USA). For the creation of clustering heatmaps, z scores were applied to normalize the data, which were then visualized through the heatmap package. Figures were produced using Origin 2021 software.

Results

Morphological and physiological changes in *X. spinosum* parasitized by *C. australis*

Figure 1A shows a partial photograph of *C. australis* parasitizing the stem of *X. spinosum* and a comparison of the seed production of *X. spinosum* during the withering period. Compared with uninfected plants, *C. australis*-infected *X. spinosum* plant height, stem thickness, leaf number and seed quantity were obviously lower (Fig. 1B). Among those factors, plant height decreased by 33.3%, stem thickness decreased by 7.75%, and leaf number and seed quantity decreased by 53.3% and 92.07%, respectively. Notably, in infected plants, the decrease in the number of seeds was much more pronounced (12.6-fold) than the decrease in other plant organs (1.1- to 2.1-fold).

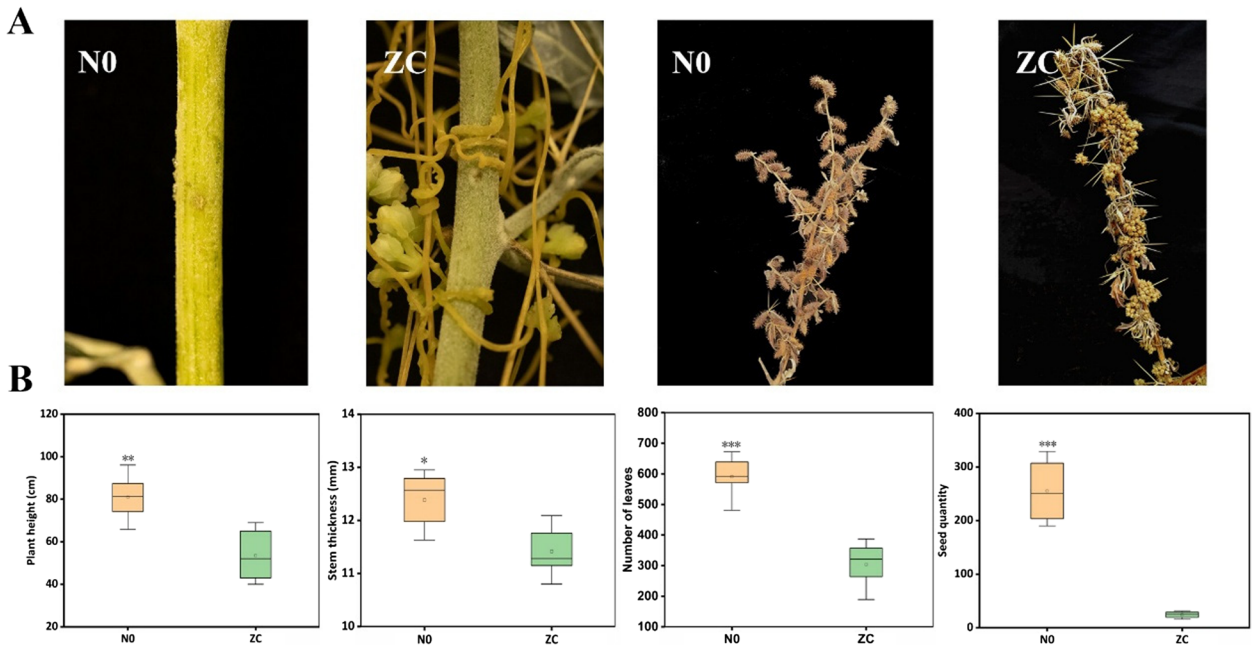

Fig. 1 Morphological changes in *X. spinosum* parasitized by *C. australis*. (**A**) Images of the sampling location and comparison of seed quantity during the harvest period. (**B**) Changes in the morphological characteristics of *X. spinosum* during parasitization. * represents the significance level at $P < 0.05$, ** represents $P < 0.01$, and *** represents $P < 0.001$

Independent-samples t tests revealed significant differences between the two groups (P value for a two-tailed test < 0.05) (Table 1). This means that *C. australis* invasion can effectively alleviate the reproduction and spread of *X. spinosum* and reduce harm to plant ecosystems and agricultural production caused by *X. spinosum*. We also measured the activities of CAT, POD, and SOD to investigate the physiological changes in both parasitized and unparasitized stems (Fig. 2). The antioxidant enzyme activity was elevated in parasitized stems, with the increase in CAT activity induced by *C. australis* being more pronounced than the increases in POD and SOD activities, demonstrating a 20.51% increase. Additionally, a slight (nonsignificant) increase in SOD activity was observed across the various treatments.

Metabolomic analyses of *X. spinosum* in response to *C. australis* parasitization

Overview

To analyze the local metabolic changes at the site of dodder contact with the stem, we performed untargeted metabolome analysis of stem samples from unparasitized and parasitized plants. Using this method, we detected 6628 metabolites in the tested samples. The unsupervised principal component analysis (PCA) results (Fig. 3A) revealed a clear separation between the parasitized and unparasitized groups in the PCA score plot. The correlation analysis between samples revealed good repeatability within the sample group (Supplementary Fig. S1). Additionally, the p value for Duncan's t test ($P < 0.05$) and the VIP values for OPLS-DA plots (VIP > 1) served as criteria for identifying metabolic differences (Fig. S2). We used goodness of fit (R2) and predictive performance (Q2) to describe the OPLS-DA model quality, and the results revealed that the model was reliable (Fig. 3B).

Table 1 Statistical analysis of morphological and physiological characteristics

Properties	F	*P*-value	t	Degree of freedom (df)	*P*-value for a two-tailed test
Plant height	0.099	0.759	4.303	10	0.002
Stem thickness	0.093	0.767	3.497	10	0.006
Leaf number	0.114	0.743	7.310	10	0.000
Seed quantity	6.717	0.027	11.445	10	0.000
CAT enzyme	1.294	0.299	−1.999	6	0.092
POD enzyme	0.095	0.769	−4.251	6	0.005
SOD enzyme	0.206	0.666	−0.360	6	0.731

Differentially expressed metabolite identification

A total of 658 differentially accumulated metabolites (DAMs), including 343 significantly upregulated DAMs and 315 significantly downregulated DAMs, in stems were screened according to the following criteria: VIP > 1.0, FC > 2 or FC < 0.5, and $P < 0.05$ (Fig. 3C; Fig. S3). The top five types of DAMs were lipids and lipid-like molecules, organic oxygen, organic acids and derivatives, phenylpropanoids and polyketides, and organoheterocyclic compounds (Fig. 3D). According to the KEGG database alignment, 11 metabolic pathways were significantly enriched ($P < 0.05$) (Fig. 3E). The main pathways enriched with DAMs included glycerophospholipid metabolism, phenylpropanoid biosynthesis, galactose metabolism, ascorbate and aldarate metabolism, lysine degradation, ABC transporters, and phenylalanine metabolism. The significantly altered DAMs within these pathways are shown in Supplementary material Table S3. The results revealed that many significantly altered pathways were related to the metabolism of lipids and lipid-like molecules, including those involved in glycerophospholipid metabolism; cutin, suberin and wax biosynthesis; and linoleic acid metabolism. Among the significantly enriched pathways in stems ($P < 0.05$), those involving organooxygen and organic acid compounds were activated. The accumulation of different phenolic compounds

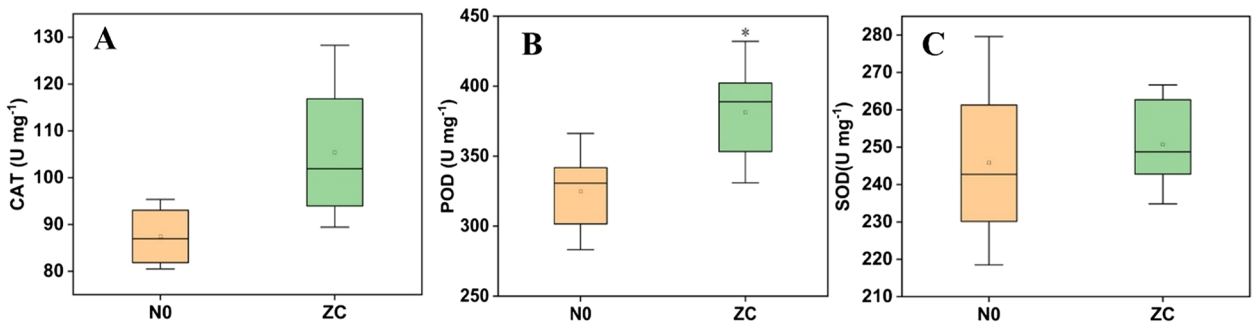

Fig. 2 Physiological changes in *X. spinosum* parasitized by *C. australis*. (**A**) Changes in CAT activity in *X. spinosum* stems under parasitization. (**B**) Changes in POD activity in parasitized *X. spinosum* stems. (**C**) Changes in SOD activity in *X. spinosum* stems under parasitization

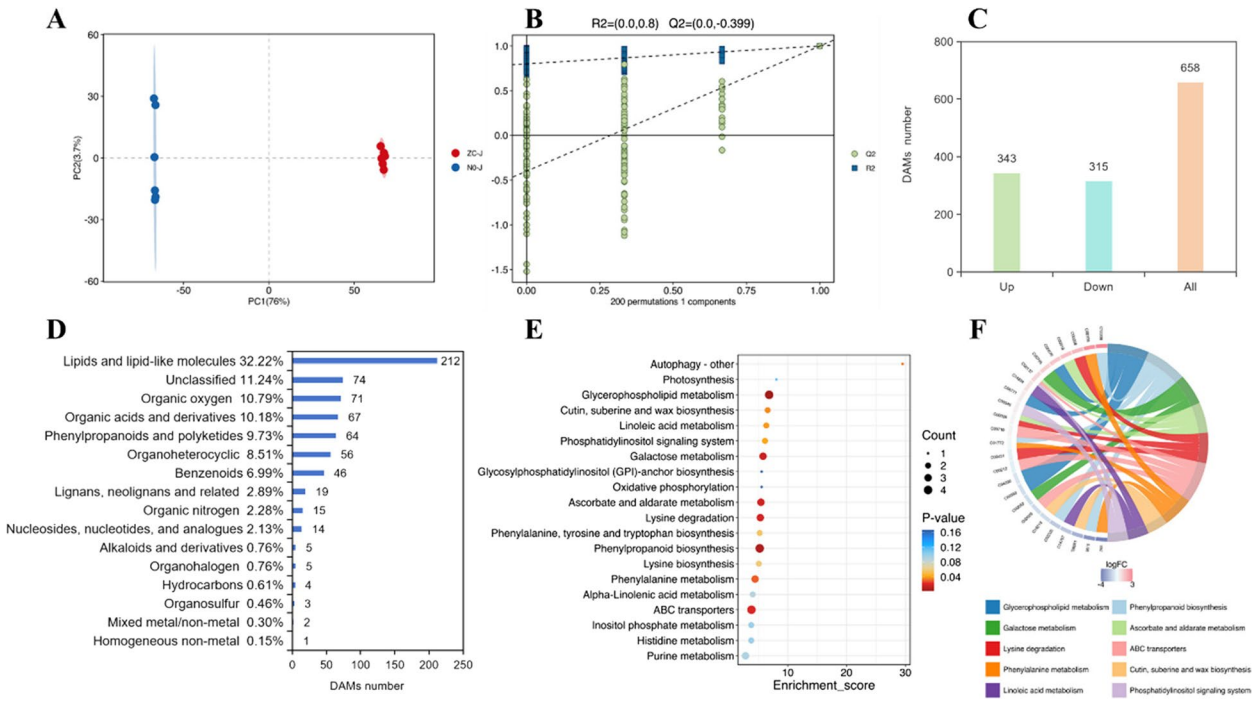

Fig. 3 Metabolome of stems under *C. australis* stress. (**A**) PCA data of metabolome samples; each point represents one sample, and different colors represent different groups. (**B**) Permutation test diagram of the OPLS-DA model. (**C**) The number of DAMs. (**D**) Bar chart of the DAMs and classification statistics. (**E**) Metabolic pathway enrichment analysis of differentially abundant metabolites was performed via the KEGG database. The top 20 KEGG pathways with the smallest *P* values were selected for display. (**F**) Chord diagram of the main KEGG signaling pathways associated with gene enrichment. The abscissa represents the enrichment score, and the ordinate represents the top 20 terms. When the z score>0, there are more increased DAMs than decreased DAMs involved in this pathway, and this pathway is more likely to be activated. Conversely, when the z score<0, there are fewer increased DAMs involved in this pathway than decreased DAMs, and this pathway is more likely to be inhibited

involved in phenylpropanoid biosynthesis was decreased (Table S2). In addition, a chord plot revealed that galactose metabolism, ascorbate and aldarate metabolism, lysine degradation, and phenylalanine metabolism were activated, whereas cutin, suberin, and wax biosynthesis was inhibited (Fig. 3F). In short, *C. australis* parasitizes *X. spinosum* and impacts various metabolic pathways through the regulation of glycerophospholipids, phenols, and organooxygen compounds, ultimately influencing plant development and growth.

Transcriptome analyses of *X. spinosum* in response to *C. australis* parasitization

Overview

Transcriptome analysis provides insight into functional genes and signaling pathways involved in plant growth and development, especially for species without reference genomes. There is currently no reference genome for *X. spinosum*, and de novo assembly has been performed using model species data. The statistical results of the transcriptome sequencing of the samples and the annotation results are shown in Table S3 and Table S4. The correlation of gene expression between samples is crucial for assessing the reliability of the database and the rationality of sample selection. PCA was used to discern the intersample differences (Fig. 4A). A heatmap showing the Spearman correlation coefficients among the samples is shown in Fig. S4. The strong correlation observed among the three biological replicates for each sample underscores the robustness of the generated transcriptomics data.

Differentially expressed gene analysis

To obtain significantly differentially expressed genes (DEGs), the screening conditions were set as follows: q value < 0.05 and difference multiple |FC|> 2. A total of 25,758 DEGs were detected in the stem, as shown in Fig. 4B. The number of upregulated genes was far greater than the number of downregulated genes. These DEGs were visualized using a volcano plot (Fig. 4C). A heatmap of the top 20 DEGs (top 10 upregulated DEGs and top 10 downregulated DEGs) was generated using public databases, including the NR, GO, KOG, Swiss-Prot, and KEGG databases, for each group, as shown in Fig. S5. The majority of the DEGs were annotated as hypothetical proteins or proteins with unknown functions. Based

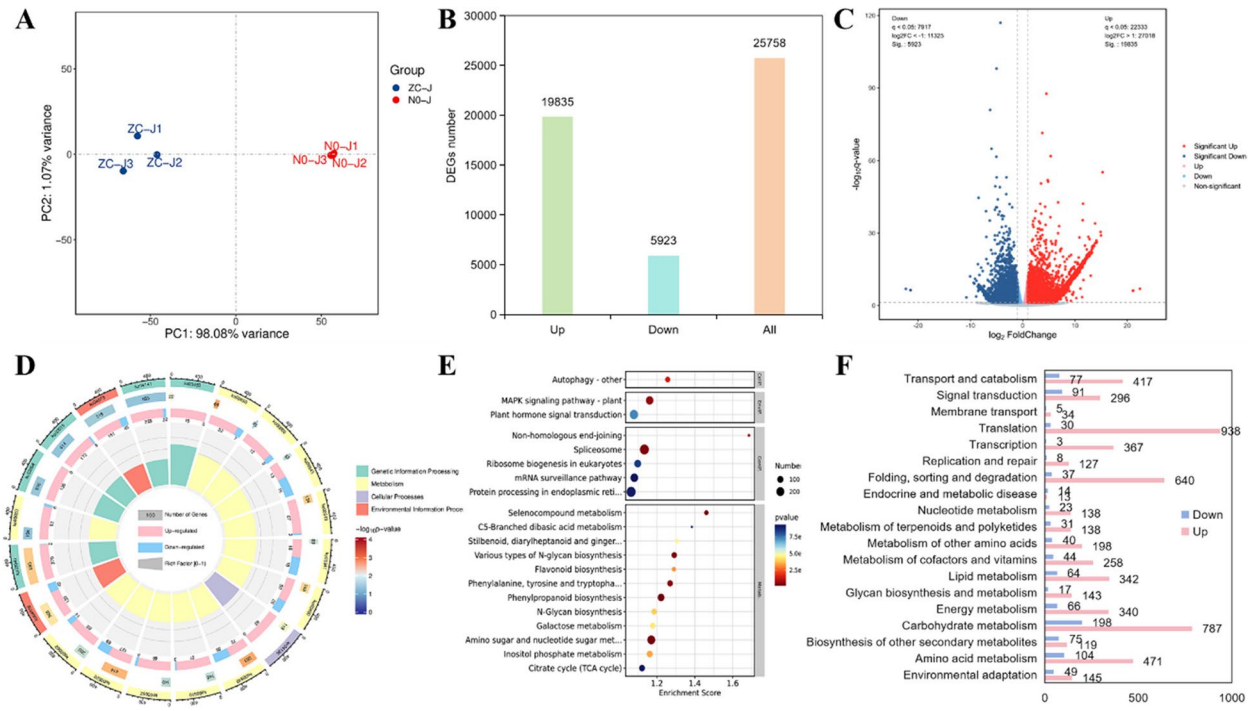

Fig. 4 Qualitative and quantitative analysis of transcriptomics data. (**A**) The PCA score chart. (**B**) Histogram showing the number of DEGs. (**C**) Volcano plot illustrating DEGs between the two groups. (**D**) The circle plot illustrates the DEGs within each category of GO enrichment. The outermost circle represents the enriched classifications. The second circle displays both the number of background genes and the q value associated with each GO term. The third circle depicts the counts of upregulated and downregulated genes. Finally, the fourth circle shows the enrichment factor for each GO term, defined as the ratio of the number of DEGs within the GO term to the number of background genes; each cell of the background auxiliary line corresponds to a value of 0.2. (**E**) Bubble chart of the top 20 most enriched KEGG pathways. (**F**) Distribution profiles for upregulated or downregulated DEGs according to the KEGG level 2 horizontal distribution comparison chart

on the GO analysis, DEGs were enriched in functions related to the extracellular region, plant-type secondary cell wall biogenesis, cell wall, cellulose binding, and cytoplasmic translation (Fig. 4D, S6). A KEGG bubble chart was generated to illustrate the outcomes of the enrichment analysis of DEGs in KEGG pathways (Fig. 4E). Specifically, DEGs in the stems were significantly enriched in a total of 14 pathways ($P < 0.05$) (Supplementary Table S5). DEGs were enriched mostly in pathways such as phenylpropanoid biosynthesis, amino sugar and nucleotide sugar metabolism, the spliceosome, and the MAPK signaling pathway-plant, among others. Notably, the downregulated genes were enriched primarily in carbohydrate metabolism and amino acid metabolism, including amino sugar and nucleotide sugar metabolism and inositol phosphate metabolism. Conversely, upregulated genes were enriched predominantly in processes such as translation, folding, sorting and degradation and carbohydrate metabolism (Fig. 4F).

Integrated analysis of the metabolome and transcriptome

By combining metabolomic and transcriptomic data, we identified the crucial pathways through which *C. australis* parasitism hampers the vegetative growth and reproductive success of *X. spinosum*, especially in terms of phenylpropanoid biosynthesis, galactose metabolism and autophagy (Fig. 5).

Phenylpropanoid biosynthesis

Phenylpropanoid biosynthesis was identified as a critical pathway by which *C. australis* parasitism inhibited *X. spinosum* growth, and Fig. 6A shows a proposed general layout with the information in the KEGG database. In this pathway, we identified 4 DAMs and 130 DEGs associated with coumarinate and lignin biosynthesis; these results were visualized and analyzed using heatmaps. The enzymes encoded by these genes include phenylalanine ammonia-lyase (PAL), 4-coumarate CoA ligase (4 CL), cinnamoyl-CoA reductase (CCR), cinnamyl-alcohol dehydrogenase (CAD), and shikimate O-hydroxycinnamoyl transferase (HCT). Among the genes encoding PAL, the expression of most was downregulated, whereas the expression of the *TRINITY_DN28489_c0_g1_i3_6* (NR id: XP_031126131.1) gene was significantly upregulated (14,831-fold) under *C. australis* stress (Table S6). These findings suggest that the PAL enzyme plays a

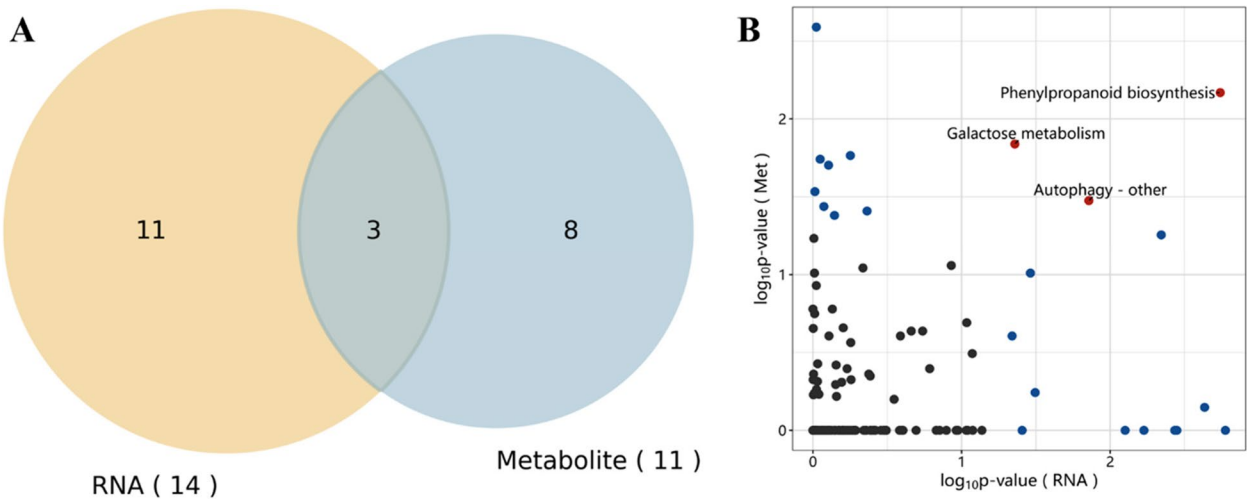

Fig. 5 KEGG pathway analysis of integrated metabolome and transcriptome results. (**A**) Ven diagram showing the number of enriched shared pathways. (**B**) Scatter plot of enriched pathways. The horizontal and vertical axes represent the -log10 (*P* value) of the two groups, with larger values indicating greater significance. The gray pathways were not significant in either omics analysis, whereas the blue pathways were significant in only one omics analysis ($P < 0.05$). In contrast, the red pathways were significant in both omics analyses ($P< 0.05$)

complex role in plant growth, development, and response to environmental stress. Trans-2-hydroxy-cinnamate and ρ-coumaroylquinic acid are key substrates required for the formation of coumarinate and lignin, and their accumulation increases under the action of PAL. Gene set enrichment analysis (GSEA) revealed that the enrichment score (ES) was −0.359, suggesting that phenylpropanoid biosynthesis negatively regulates the growth of *X. spinosum* under *C. australis* stress (Fig. 6B). Notably, the core gene set is located on the right side of the peak. Figure 6C shows the correlations between the top 20 DEGs and DAMs. The expression levels of genes encoding HCT were significantly correlated with the levels of p-coumaroylquinic acid, indicating that the HCT gene promotes the accumulation of lignin. The CCR and CAD genes are located in the later steps of lignin biosynthesis, but they are directly related to lignin synthesis. The downregulation of the expression of genes encoding the CCR and CAD enzymes led to reduced saponin aldehyde and sinapyl alcohol contents (87.83% and 63.69%, respectively), which are involved in lignin synthesis as upstream substances. Overall, these results revealed that *C. australis* inhibited lignin accumulation in *X. spinosum* stems, which further induced stress on plant growth and severely affected the formation of plant organs.

Galactose metabolism

X. spinosum plants under *C. australis* stress also presented an altered galactose metabolism pathway, as shown in Fig. 7A. A total of 71 DEGs associated with galactose metabolism were identified (Table S7). These genes encode enzymes involved in various aspects of galactose metabolism, including alpha-galactosidase (galA), beta-galactosidase (lacZ), hexokinase (HK), UDP-glucose 4-epimerase (galE), and phosphoglucomutase (pgm). The expression of most genes encoding these enzymes was upregulated in the parasitized plants. Conversely, the expression of UDP-galactose, which serves as the primary metabolite of galactose, was significantly downregulated. These findings clearly demonstrate that these enzymes negatively regulate UDP-galactose. The upregulation of the expression of these genes increased the D-myo-inositol and D-tagatose compound contents by 129.52% and 151.60%, respectively, compared with those in unparasitized plants. In addition to the pgm enzyme, the HK enzyme plays a role in glycolysis. D-myo-inositol and D-tagatose were positively correlated with most genes involved in galactose metabolism, whereas UDP-galactose was significantly negatively correlated (Fig. 7C).

Autophagy—other

A total of 60 DEGs encoding proteins involved in autophagy were identified (Table S8); these genes, which regulate autophagy, are referred to as ATGs. ATG proteins are classified into five functional groups, as illustrated in Fig. 8A: (1) the TORC1 complex, (2) the serine/threonine-protein kinase (ATG1) complex, (3) the autophagy-specific phosphatidylinositol 3-kinase (PI3 K) complex, (4) the integral membrane protein ATG9 and the ATG2-ATG18 complex, and (5) the ATG12 conjugation system (ATG5, ATG7, ATG10,

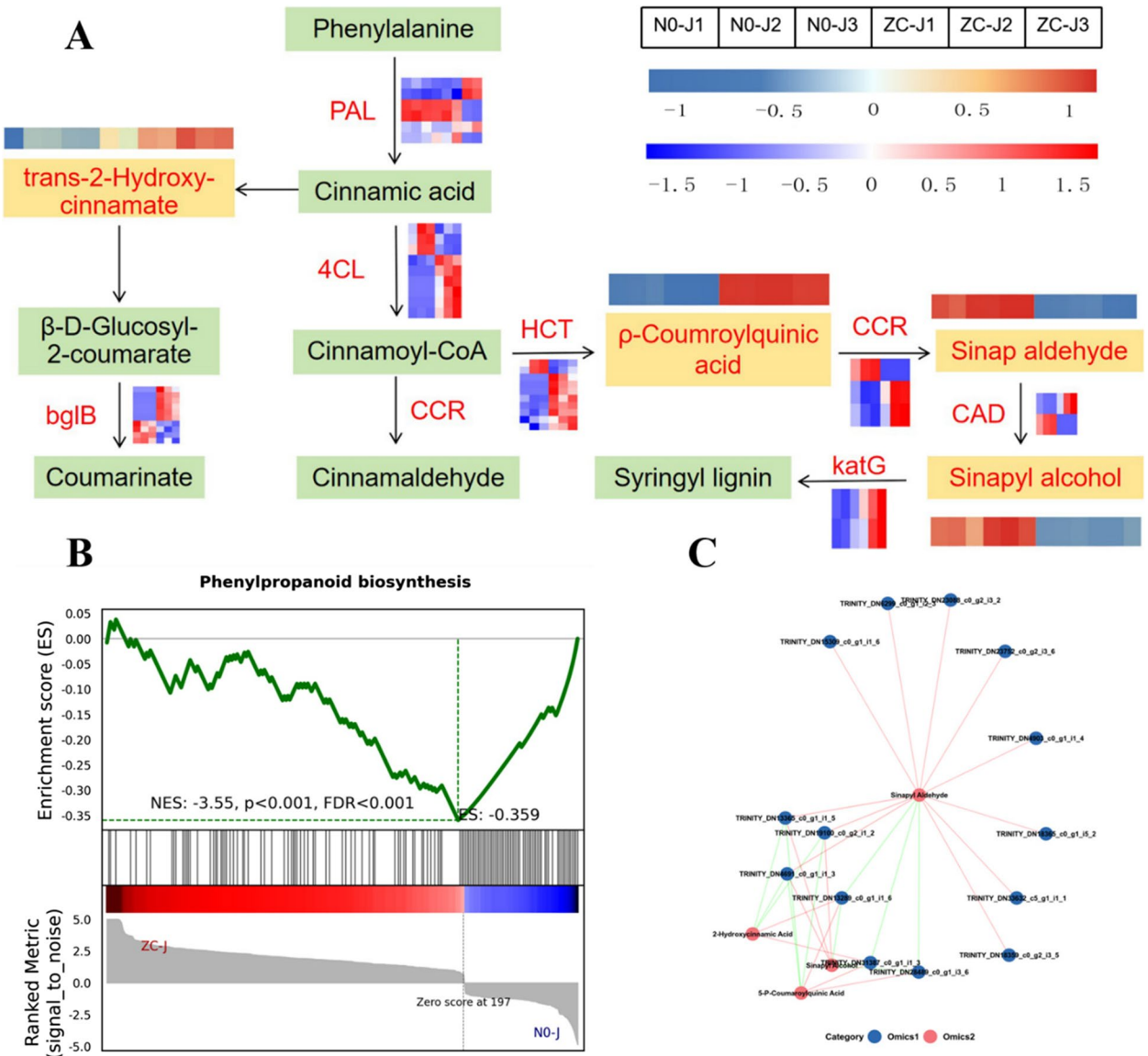

Fig. 6 Phenylpropanoid biosynthesis pathway. (**A**) Schematic diagram of phenylpropanoid biosynthesis. DAMs and DEGs are marked in red. Metabolic pathways were constructed on the basis of information in the KEGG database with some modifications. (**B**) GSEA results for the phenylpropanoid biosynthesis gene sets. The dark green line represents the enrichment score (ES) distribution for all genes. The position where the absolute value of the curve reaches its maximum on the Y-axis indicates the enrichment score for the gene set. NES > 0 indicates pathway activation, NES < 0 indicates pathway inhibition, and NES = 0 indicates no enrichment. When ES > 0, the core genes are located on the left side of the peak; conversely, when ES < 0, the core genes are found on the right side of the peak. (**C**) Network diagram of the correlations between significantly highly expressed genes and DAMs. In this diagram, the red circles represent the metabolome, and the blue circles represent the transcriptome. The red lines indicate positive correlations, whereas the green lines denote negative correlations. The thickness of the lines reflects the strength of the correlation, with thicker lines representing stronger correlations (same as below)

ATG12, and ATG16). The expression of all DEGs encoding proteins involved in autophagy regulation was upregulated. Phosphatidylethanolamine (PE) is a glycerophospholipid characterized by the presence of a phosphorylethanolamine moiety at a glycerol substitution site. The expression of PE was significantly reduced in parasitic stems, decreasing by 47.03%. Correlation analysis between PE and the top 20 DEGs involved in the autophagy pathway revealed that all DEGs were significantly negatively correlated with the relative content of PE (Fig. 8C). These results suggest that the genes encoding ATGs negatively regulate the synthesis of PE.

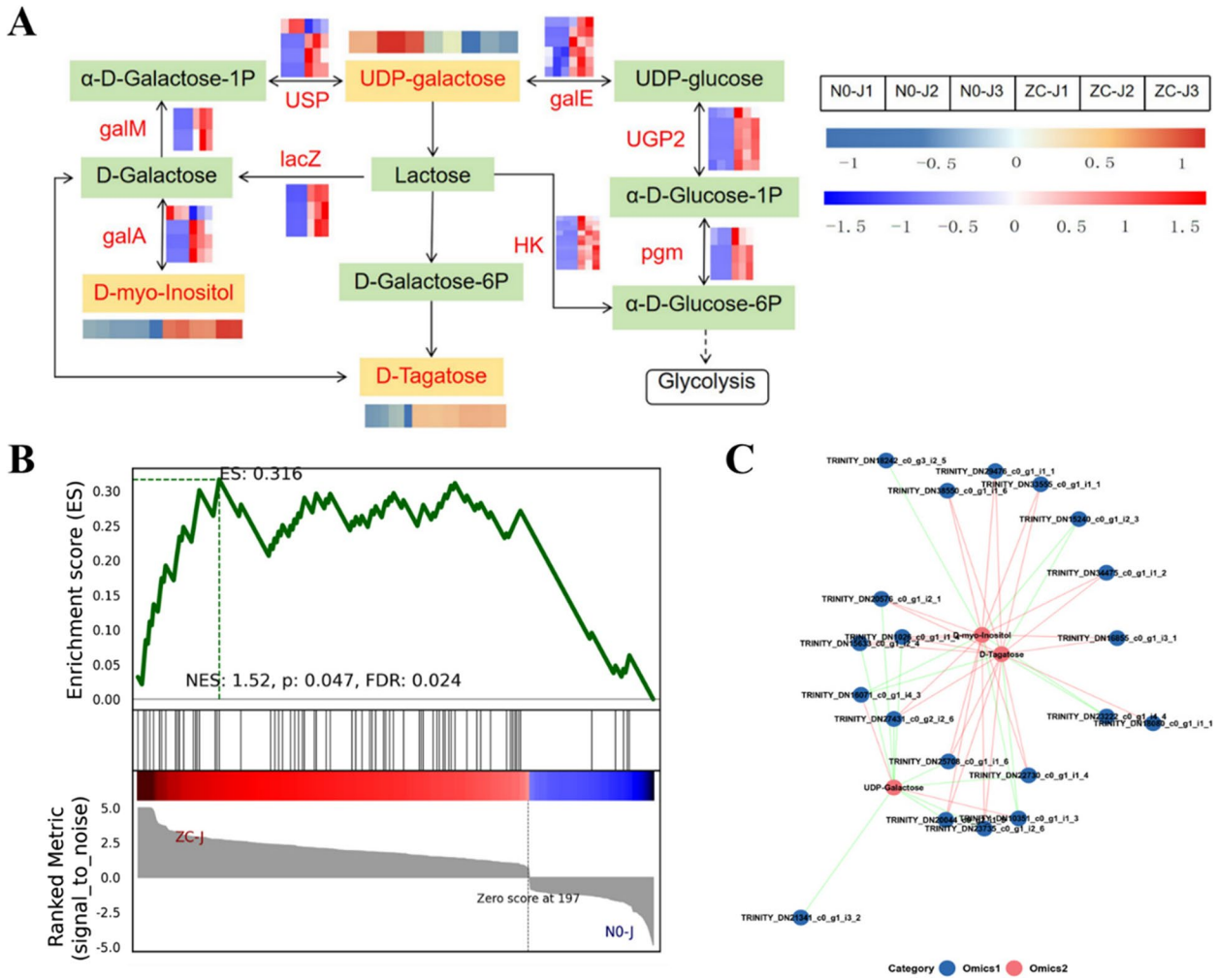

Fig. 7 Galactose metabolism pathway. (**A**) Schematic diagram of galactose metabolism. (**B**) GSEA results for the galactose metabolism gene sets. (**C**) Network diagram of the correlations between significantly highly expressed genes and DAMs

Correlation analysis of DAMs, DEGs and growth performance

The effect of DAMs related to the synthesis of lignin and galactose, and its DEGs on growth performance was further explored by Pearson correlation analysis for *X. spinosum*. First, the correlation between DAMs and related genes was analyzed (Fig. 9A). Our analysis uncovered significant correlations ($P < 0.05$) between enriched compounds and their respective genes within individual pathways. Moreover, cross-pathway analysis revealed significant associations between compounds and genes across various pathways. For example, ATGs in Autophagy—other pathway displayed significant positive correlations with DEGs encoding glaM, UGP2, HK, pgm, and lacZ in the galactose metabolism pathway, highlighting the intricate nature of cross-pathway interactions and molecular networks. Simultaneously, by correlating DAMs and DEGs with phenotypic traits of *X. spinosum* plants, it was revealed that the phenotypes showed strong positive associations with DAMs and DEGs enriched in galactose biosynthesis, lignin degradation, and autophagy pathways (Fig. 9B). This association was notably observed in the quantities of leaves and seeds, suggesting that these metabolites and genes play a positive role in regulating the growth and reproductive capacity of *X. spinosum*.

Validation of RNA-seq data by RT–qPCR

In this study, 10 indispensable DEGs related to key metabolic pathways were chosen for RT–qPCR analysis to validate the expression profiles obtained (Fig. S7). These genes are associated with phenylpropanoid biosynthesis, pentose and glucuronate interconversions and galactose metabolism. The qRT–PCR analysis revealed that the expression patterns of these genes closely matched the FPKM values obtained from sequencing in response to

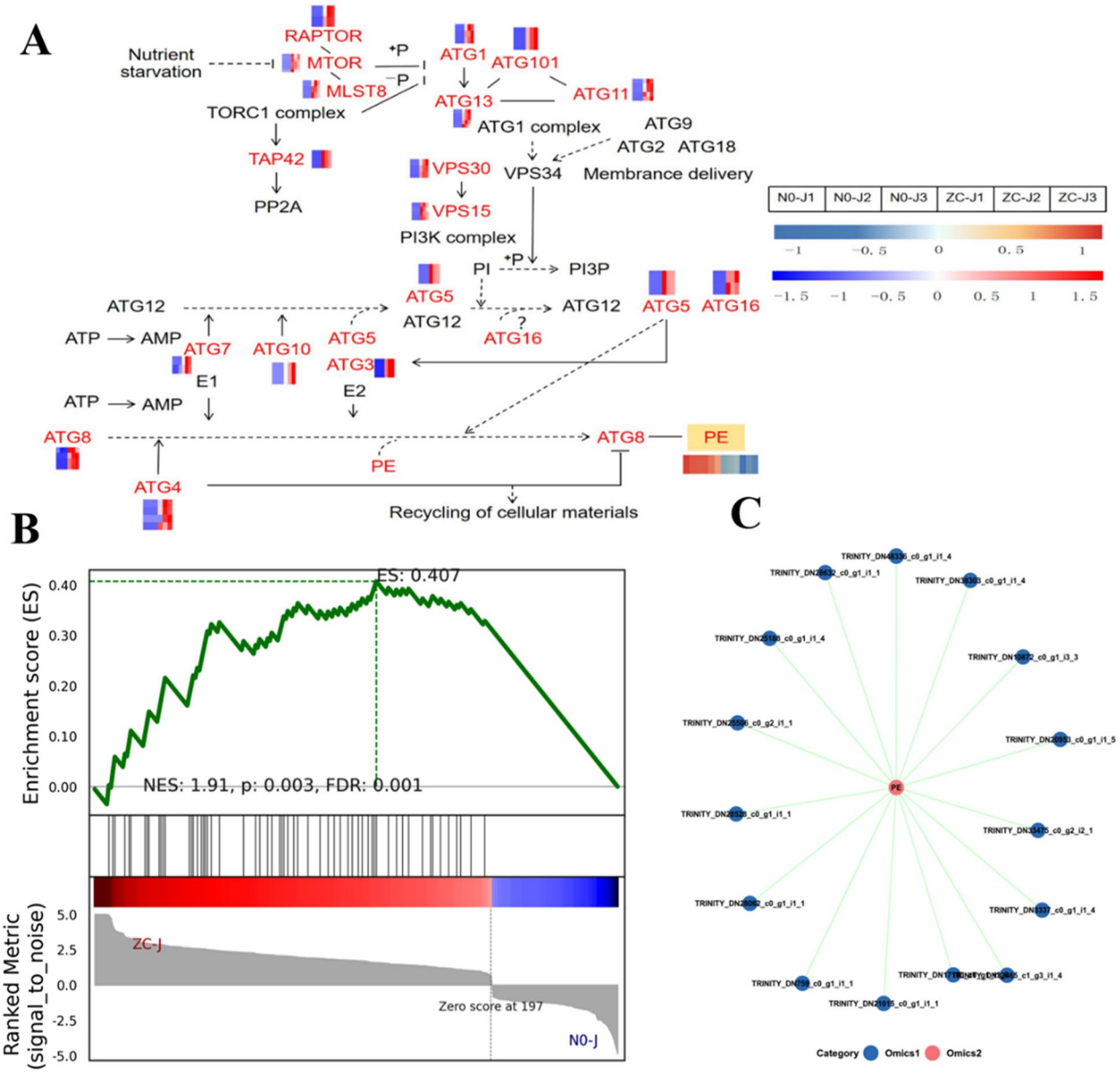

Fig. 8 Autophagy-other pathway. (**A**) Schematic diagram of the autophagy-other pathway. (**B**) GSEA results for the autophagy-other gene sets. (**C**) Network diagram of the correlations between significantly highly expressed genes and DAMs

the respective treatments, suggesting the reliability of the RNA-seq data.

Discussion

Reducing the amount of plant seeds is crucial in controlling invasive alien plants, as it helps decrease the number of populations. *Cuscuta* parasitism has been found to slow the growth of *Mikania* [20] and *Bidens pilosa* [21], inhibit organ development, and ultimately result in a decrease in seed setting. Investigating the regulatory mechanism of *Cuscuta* on the growth and reproduction of invasive alien plants is essential for the development of alternative products for controlling these invasive species. This study explored how *C. australis* inhibits the vegetative and reproductive growth of *X. spinosum* through an integrated analysis of the metabolome and transcriptome, complemented by morphologic and physiologic observations. Phenotypic changes were observed in *X. spinosum* after being treated with *C. australis*, leading to evident growth damage and a notable decrease in seed yield (Fig. 1). These findings align with those of numerous previous studies [25, 26].

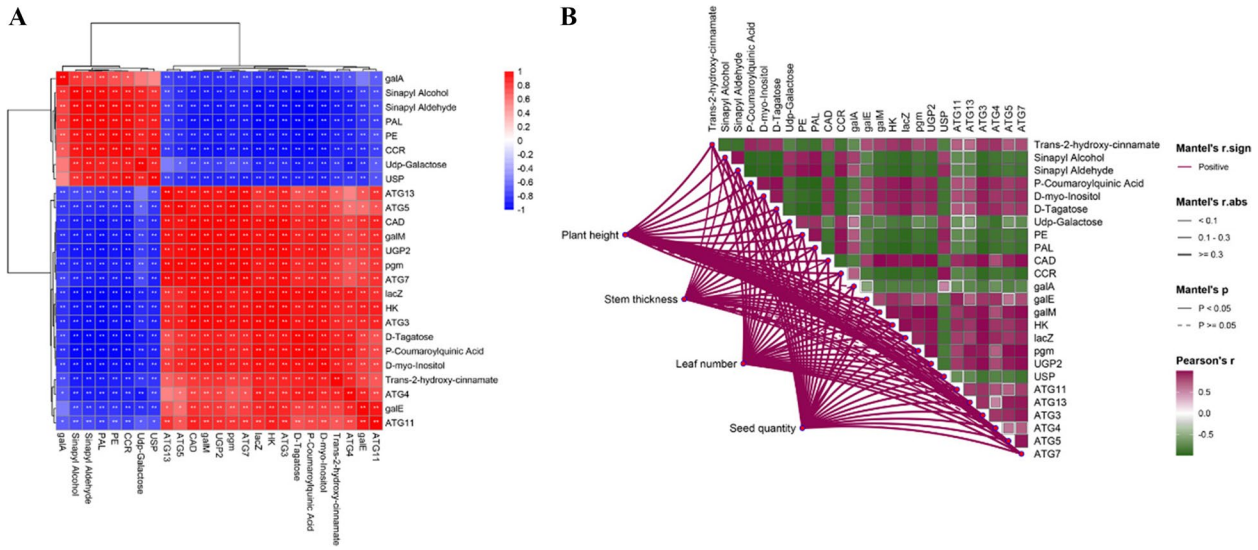

Fig. 9 Correlation analysis of DAMs, DEGs and growth performance. (**A**) Heatmap of the correlation network of of DEGs and DAMs in three pathways. Red colour indicates positive correlation and blue colour indicates negative correlation. (**B**) Correlation of DEGs and DAMs with growth traits. Units are based on red for positive correlation and green for negative correlation. Red lines indicate positive correlation and green indicates negative correlation

C. australis regulates the defense response of *X. spinosum* by stimulating antioxidant enzyme activity

SOD, POD, and CAT are essential enzymes in the antioxidant defense system that play crucial roles in eliminating specific reactive oxygen species (ROS), regulating oxygen levels, and protecting the cell membrane from damage [27–31]. Research has indicated that the activities of most antioxidant enzymes tend to increase in response to stressful conditions [32]. The peroxidase activity in parasitized *X. spinosum* stems increased, with a particularly noticeable increase in POD enzyme activity. The increased antioxidant enzyme activity indicates that a defense system was activated by *C. australis*. The activity of CAT in plant tissues is closely linked to plant stress resistance. CAT is not a stable enzyme and can increase in high hydrogen peroxide (H_2O_2) conditions resulting from stress. These findings indicate that *C. australis* parasitism may affect the function of CAT, leading to the accumulation of ROS, causing cells to be poisoned by H_2O_2, ultimately affecting the normal growth of plants [33, 34].

C. australis parasitism suppresses lignin synthesis through the phenylpropanoid pathway to hinder *X. spinosum* growth and development

The phenylpropanoid pathway produces a variety of compounds, such as coumarins and lignins, and is a general strategy for plant defense against biotic stress [35]. In the present study, *C. australis* parasitism increased the expression levels of trans-2-hydroxy-cinnamate and ρ-coumaroylquinic acid, which are essential substrates for the production of coumarin. PAL is a crucial enzyme that regulates coumarin synthesis. The expression of the gene encoding the PAL enzyme was both upregulated and downregulated, highlighting the complexity of the role of PAL in the phenylpropanoid pathway. The upregulation of PAL expression results in a dwarf phenotype in *Ricinus communis* L. [36]. These findings suggest that PAL may negatively regulate the growth of parasitized plants. Lignin, the second most abundant polymer on Earth, primarily accumulates in the cell wall of plants; it serves multiple functions, such as providing mechanical support, facilitating water and mineral transport, and assisting in the defense against pathogen invasion [37]. The expression of most genes related to the lignin pathway (such as CCR and CAD) were downregulated in parasitized *X. spinosum*. CCR is the first key enzyme in the specific pathway of lignin synthesis, and CAD serves as the pivotal enzyme in the biosynthesis of monolignols prior to the oxidative polymerization of the cell wall [38]. The downregulation of the expression of genes encoding CCR and CAD enzymes results in decreased levels of sinapaldehyde and sinapyl alcohol (Fig. 6), which serve as upstream precursors in lignin synthesis. This finding suggests that the biosynthesis of lignin may be inhibited during the parasitism process of *C. australis*.

C. australis parasitism leads to an increase in sugar accumulation through galactose metabolism, resulting in glucose metabolism disorders

Galactose metabolism is the biochemical process of converting galactose to glucose for use in energy metabolism [39]. Galactose is a key component of cell wall polymers, glycolipids, and glycoproteins, with UDP-galactose serving as its primary metabolite. UDP-glucose, a nucleotide sugar, functions primarily as a donor of glucose residues in glycosylation reactions and is essential for the biosynthesis of sucrose and various polysaccharides, including cellulose, hemicellulose, and pectin [40]. galE catalyzes the interconversion between UDP-galactose and UDP-glucose [41]. The expression of the genes encoding the galE enzyme was upregulated, resulting in reduced galE epimerase activity. This reduction in activity leads to the accumulation of UDP-galactose; however, excessive levels of UDP-galactose may be detrimental to plant growth and development [42]. The HK enzyme is a signaling molecule in plants that regulates and controls growth and development; it functions as an indispensable bifunctional enzyme within these organisms. The loss of HK function can delay plant aging. However, following the overexpression of the hexokinase gene, plant growth is inhibited, and the rate of aging accelerates [43]. In tomato plants that overexpress hexokinase, the senescence rate increases, whereas the chlorophyll content and photosynthetic rate in the leaves decrease [44]. In this study, the expression of genes encoding HK was upregulated in stems affected by *C. australis* parasitism, which inhibited *X. spinosum* growth and development. Pgm is an enzyme that catalyzes glycolysis [45]. *C. australis* inhibits pgm enzyme activity through the upregulation of the expression of specific genes, further obstructing glycolysis, which can have detrimental effects on plants. In summary, *C. australis* parasitism induces the upregulation or downregulation of the expression of genes encoding enzymes that regulate the metabolism of glucose, fructose, galactose, and other sugars; this results in abnormalities in the structure, function, and concentration of these enzymes, leading to increased sugar accumulation in *X. spinosum* and causing disorders in sugar metabolism. Ultimately, this disruption adversely affects the vegetative growth and reproductive performance of *X. spinosum*.

C. australis parasitism induces excessive autophagy through the upregulation of the expression of autophagy-related genes (*ATGs*), leading to the accelerated aging of *X. spinosum*

Autophagy refers to the process by which cells encapsulate portions of their own cytoplasm to form autophagosomes, which are subsequently digested and degraded by hydrolases within lysosomes or vacuoles [46]. Nutrient starvation is a well-established experimental condition used to induce autophagy [47]. Autophagy functions as a cytoprotective and prosurvival mechanism; however, excessive autophagy promotes cell death [48]. Nearly all the autophagy-deficient mutants were able to complete their normal life cycle, but they exhibited early leaf senescence, which was further exacerbated under nutrient-deficient conditions [49]. *ATGs* and autophagy-regulating kinases are important components of the autophagy process [50]. Environmental stress activates signaling pathways by upregulating the expression of genes encoding serine/threonine protein (MTOR) kinases, which subsequently affect the ATG1/ATG13 complex to initiate autophagy [47]. *C. Australis* significantly increased the expression of all the autophagy-related genes involved in this pathway, particularly ATG7, ATG5, and all the ATG8 homologs. These findings suggest that *C. australis* enhances the formation of the ATG8-PE system. PE acts as a positive regulator of autophagy [51]; however, autophagy competes with other PE-consuming processes for the available phospholipid pool, indicating that PE may be a limiting factor for autophagy [52]. The decrease in PE compounds in this study may have inhibited autophagy. In *Arabidopsis thaliana*, loss-of-function ATG6 mutants present short stature, short roots, premature senescence, and low fertility (flowers and seeds) [53]. *C. australis* parasitizes *X. spinosum* and obtains nutrients through haustoria, resulting in a nutritional starvation state of *X. spinosum* that activates the autophagy pathway. As the duration of parasitism increases, nutrient deficiency in *X. spinosum* results in excessive autophagy and premature plant senescence. This process significantly impairs the nutrient absorption of *X. spinosum*, ultimately affecting both seed yield and seed performance.

In summary, the phenylpropanoid biosynthesis pathway is a cornerstone of plant secondary metabolism, producing critical compounds such as flavonoids and lignin. These metabolites play pivotal roles in plant defense mechanisms, developmental processes, and environmental adaptation, directly influencing stress resistance and overall growth [54]. The galactose metabolism pathway serves dual functions in energy provision and carbon source replenishment. Galactose, derived from the breakdown of cell wall polysaccharides, acts as an alternative energy reserve during carbon limitation and participates in sugar-sensing pathways, including the target of rapamycin (TOR) signaling network, which modulates growth and development [55]. Moreover, the autophagy pathway functions as a master regulator of cellular homeostasis. By selectively degrading and recycling damaged organelles or macromolecules, autophagy sustains

cell viability under nutrient deprivation, senescence, or pathogen challenge, making it a fundamental adaptive strategy in dynamic environments. Notably, these three pathways are functionally interconnected, forming a metabolic continuum of"synthesis–degradation–reutilization."Phenylpropanoid biosynthesis consumes carbon skeletons, galactose metabolism replenishes carbon skeletons, and autophagy ensures efficient carbon recycling, maintaining metabolic equilibrium [56, 57]. The disruption of any of these pathways leads to pronounced phenotypic consequences, including growth retardation, premature aging, and altered sugar sensitivity, underscoring their biological importance. The three metabolic pathways and key genes identified in this study reveal potential inhibitory sites for *C. australis* parasitism. These findings provide a foundation for the development of targeted biopesticides through RNA interference (RNAi) technology [58, 59]. RNAi constructs that silence essential *X. spinosum* genes can lead to highly specific gene suppression, offering an efficient and environmentally sustainable strategy for controlling the spread of *X. spinosum*. The multiomics method utilized in this study is a cutting-edge strategy to study the mechanisms by which external factors inhibit the growth and reproduction of invasive plants. The three key metabolic pathways and their associated genes have been validated in other species and are critical pathways affecting plant growth and development. These results highlight the strong feasibility and translational potential of our findings for practical applications. Additionally, precision-targeted pesticides developed on the basis of these discoveries offer significant ecological advantages over conventional broad-spectrum herbicides; they can selectively inhibit invasive species while protecting native vegetation, thereby maintaining biodiversity and ecological functions. However, this study is subject to several limitations. The absence of a published genome and species-specific databases for *X. spinosum* restricts the depth of integrated transcriptomic and metabolomic analyses. Future studies will prioritize genome assembly and multi-tissue transcriptome sequencing, complemented by targeted genetic manipulation, to unravel the mechanistic basis of this parasitic interaction.

Conclusion

The potential mechanism by which *C. australis* suppresses *X. spinosum* growth and reproduction likely involves its interference with the host's antioxidant enzyme system, leading to developmental constraints. Our integrated pathway analysis of metabolomic and transcriptomic data shows *C. australis* parasitism mediates growth and reproductive suppression in *X. spinosum* through coordinated disruption of phenylpropanoid biosynthesis, galactose metabolism and autophagy pathways. While our data showed *C. australis*'s interference with these pathways, targeted functional experiments remain essential to validate their causal roles in the observed phenotypic suppression.

Supplementary Information

The online version contains supplementary material available at https://doi.org/10.1186/s12870-025-06698-1.

Supplementary Material 1.

Supplementary Material 2.

Acknowledgements
We sincerely acknowledge Marcelo Sternberg for proofreading the manuscript.

Clinical trial number
Not applicable.

Authors' contributions
X.W. designed the experiments and managed the project. Y.W., H.B. and X.G. performed the data analyses. Y.W. and H.B wrote the manuscript. All authors discussed the results and commented on the manuscript. All authors read and approved the contents of this paper.

Funding
This study was supported by the "Investigation on the occurrence and spread risk of agricultural alien invasive species" from the Ministry of Agriculture and Rural Affairs of China (13220160).

Data availability
The RNA sequence data reported in this paper have been deposited in the Genome Sequence Archive (Genomics, Proteomics & Bioinformatics 2021) in National Genomics Data Center (Nucleic Acids Res 2022), China National Center for Bioinformation/Beijing Institute of Genomics, Chinese Academy of Sciences (GSA: CRA020087). Metabolomics data are accessible in GSA (OMIX007767). All data analyzed during this study are included in this published article (and its supplementary information fles).

Declarations

Ethics approval and consent to participate
Not applicable.

Consent for publication
Not applicable.

Competing interests
The authors declare no competing interests.

Received: 29 October 2024 Accepted: 8 May 2025
Published online: 17 May 2025

References

1. Fukasawa K, Miyashita T, Hashimoto T, Tatara M, Abe S. Differential population responses of native and alien rodents to an invasive predator, habitat alteration and plant masting. Proc R Soc B: Biol Sci. 2013;280:20132075.
2. Rocchia E, Luppi M, Paradiso F, Ghidotti S, Martelli F, Cerrato C, et al. Distribution drivers of the alien butterfly geranium bronze (*Cacyreus marshalli*)

in an Alpine protected area and indications for an effective management. Biology. 2022;11: 563.
3. Jiang Z, Wang Y, Zheng Y, Cai M, Peng C, Li W. Physiological and transcriptomic responses of *Mikania micrantha* stem to shading yield novel insights into its invasiveness. Biol Invasions. 2021;23:2927–43.
4. Schaffner U, Steinbach S, Sun Y, Skjøth CA, de Weger LA, Lommen ST, et al. Biological weed control to relieve millions from *Ambrosia* allergies in Europe. Nat Commun. 2020;11:1745.
5. Liu X, Blackburn TM, Song T, Wang X, Huang C, Li Y. Animal invaders threaten protected areas worldwide. Nat Commun. 2020;11:2892.
6. Mu C, Guo X, Chen Y. Impact of global climate change on the distribution range and niche dynamics of *Eleutherodactylus planirostrish* in China. Biology. 2022;11: 588.
7. Yuan Z, Zheng X, Zhao Y, Liu Y, Zhou S, Wei C, et al. Phytotoxic compounds isolated from leaves of the invasive weed *Xanthium spinosum*. Molecules. 2018;23: 2840.
8. Martin RJ, Carnahan JA. The effect of field storage and laboratory conditions on germination of five *Xanthium* species. Aust J Agric Res. 1983;34:249–60.
9. McRae CF, Auld BA. The influence of environmental factors on anthracnose of *Xanthium spinosum*. Phytopathology. 1988;78:1182–6.
10. Auld BA, Say MM. Comparison of isolates of *Colletotrichum orbiculare* from Argentina and Australia as potential bioherbicides for *Xanthium spinosum* in Australia. Agr Ecosyst Environ. 1999;72:53–8.
11. Du Z, Xu W, Yan P, Wang S, Guo Y. Three newly recorded alien invasive plants of *Xanthium* in Xinjiang. Xinjiang Agric Sci. 2012;49:879.
12. Hocking PJ, Liddle MJ. The biology of Australian weeds: 15. Xanthium occidentale Bertol. complex and Xanthium spinosum L. 1986.
13. Auld BA, McRae CF, Say MM. Possible control of *Xanthium spinosum* by a fungus. Agr Ecosyst Environ. 1988;21:219–23.
14. Andreani S, Paolini J, Costa J, Muselli A. Chemical composition of essential oils of *Xanthium spinosum* L., an invasive species of corsica. Chem Biodiversity. 2017;14:e1600148.
15. Li J, Ma M. Seeds over-wintering characteristics of Italian Cocklebur and Stab Cocklebur: two invasive plants in Xinjiang, China. South African journal of botany. 2019;121:216–8.
16. Wang P, Ma S, Li L, Li Y, Qu J, Yu S. Humulane-type and germacrane-type sesquiterpenoids from the fruits of *Xanthium spinosum* Linn. Phytochemistry. 2021;189: 112818.
17. Tao Y, Shang T, Yan J, Hu Y, Zhao Y, Liu Y. Effects of sand burial depth on *Xanthium spinosum* seed germination and seedling growth. BMC Plant Biol. 2022;22:43.
18. Hilgendorf JH, Goeden RD. Phytophagous insect faunas of spiny clotbur, *Xanthium spinosum*, and cocklebur, *Xanthium strumarium*, in southern California. Environ Entomol. 1983;12:404–11.
19. Liu Y, Liu L, Zhao W, Guan Z, Jiang J, Fang W, et al. A transcriptional response atlas of *Chrysanthemum morifolium* to dodder invasion. Environ Exp Bot. 2021;181: 104272.
20. Yu H, Yu F, Miao S, Dong M. Holoparasitic *Cuscuta campestris* suppresses invasive *Mikania micrantha* and contributes to native community recovery. Biol Cons. 2008;141:2653–61.
21. Yang B, Li J, Zhang J, Yan M. Effects of nutrients on interaction between the invasive *Bidens pilosa* and the parasitic *Cuscuta australis*. Pak J Bot. 2015;47:1693–9.
22. Zhang Z. Evolution of ecological damage probability in the arid area based on SPCA: a case study of Yinchuan City. 2024.
23. Zhao S, He L, Lu Y, Duo L. The impact of modified nano-carbon black on the earthworm *Eisenia fetida* under turfgrass growing conditions: assessment of survival, biomass, and antioxidant enzymatic activities. J Hazard Mater. 2017;338:218–23.
24. Rehman A, Weng J, Li P, Shah IH, Rahman S ur, Khalid M, et al. Green synthesized zinc oxide nanoparticles confer drought tolerance in melon (*Cucumis melo* L.). Environ Exp Bot. 2023;212:105384.
25. Tjiurutue MC, Sandler HA, Kersch-Becker MF, Theis N, Adler LA. *Cranberry* resistance to dodder parasitism: induced chemical defenses and behavior of a parasitic plant. J Chem Ecol. 2016;42:95–106.
26. Bai W, Gao F, Feng W, Wu Q, Feng Y. The native stem holoparasitic *Cuscuta japonica* suppresses the invasive plant *Ambrosia trifida* and related mechanisms in different light conditions in northeast China. Front Plant Sci. 2022;13: 904326.
27. Naeem M, Han R, Ahmad N, Zhao W, Zhao L. Tobacco as green bioreactor for therapeutic protein production: latest breakthroughs and optimization strategies. Plant Growth Regul. 2024;103:227–41.
28. Naeem M, Shahzad K, Saqib S, Shahzad A, Nasrullah,Younas M, et al. The Solanum melongena COP1LIKE manipulates fruit ripening and flowering time in tomato (*Solanum lycopersicum*). Plant Growth Regul. 2022;96:369–82.
29. Weng J, Li P, Rehman A, Wang L, Gao X, Niu Q. Physiological response and evaluation of melon (*Cucumis melo* L.) germplasm resources under high temperature and humidity stress at seedling stage. Scientia Horticulturae. 2021;288:110317.
30. Weng J, Rehman A, Li P, Chang L, Zhang Y, Niu Q. Physiological and transcriptomic analysis reveals the responses and difference to high temperature and humidity stress in two melon genotypes. Int J Mol Sci. 2022;23: 734.
31. Li P, Yu J, Feng N, Weng J, Rehman A, Huang J, et al. Physiological and transcriptomic analyses uncover the reason for the inhibition of photosynthesis by phosphate deficiency in *Cucumis melo* L. Int J Mol Sci. 2022;23: 12073.
32. Singh R, Upadhyay AK, Chandra P, Singh DP. Sodium chloride incites reactive oxygen species in green algae *Chlorococcum humicola* and *Chlorella vulgaris*: implication on lipid synthesis, mineral nutrients and antioxidant system. Biores Technol. 2018;270:489–97.
33. Iqbal B, Ahmad N, Li G, Jalal A, Khan AR, Zheng X, et al. Unlocking plant resilience: advanced epigenetic strategies against heavy metal and metalloid stress. Plant Sci. 2024;349: 112265.
34. Ahmad N, Naeem M, Ali H, Alabbosh KF, Hussain H, Khan I, et al. From challenges to solutions: the impact of melatonin on abiotic stress synergies in horticultural plants via redox regulation and epigenetic signaling. Sci Hortic. 2023;321: 112369.
35. Naeem M, Zhao W, Ahmad N, Zhao L. Beyond green and red: unlocking the genetic orchestration of tomato fruit color and pigmentation. Funct Integr Genomics. 2023;23:243.
36. Cho S-H, Kang K, Lee S-H, Lee I-J, Paek N-C. OsWOX3A is involved in negative feedback regulation of the gibberellic acid biosynthetic pathway in rice (*Oryza sativa*). J Exp Bot. 2016;67:1677–87.
37. Beckers S, Peil S, Wurm FR. Pesticide-loaded nanocarriers from lignin sulfonates—a promising tool for sustainable plant protection. ACS Sustainable Chem Eng. 2020;8:18468–75.
38. Su X, Zhao Y, Wang H, Li G, Cheng X, Jin Q, et al. Transcriptomic analysis of early fruit development in Chinese white pear (*Pyrus bretschneideri Rehd.*) and functional identification of *PbCCR1* in lignin biosynthesis. BMC Plant Biol. 2019;19:417.
39. Hou Q, Zhang H, Zhu J, Liu F. Transcriptome analysis to identify responsive genes under sublethal concentration of bifenazate in the diamondback moth, *Plutella xylostella* (Linnaeus, 1758)(Lepidoptera: Plutellidae). Int J Mol Sci. 2022;23: 13173.
40. Althammer M, Regl C, Herburger K, Blöchl C, Voglas E, Huber CG, et al. Overexpression of UDP-sugar pyrophosphorylase leads to higher sensitivity towards galactose, providing new insights into the mechanisms of galactose toxicity in plants. Plant J. 2022;109:1416–26.
41. Balakrishnan B, An D, Nguyen V, DeAntonis C, Martini PG, Lai K. Novel mRNA-based therapy reduces toxic galactose metabolites and overcomes galactose sensitivity in a mouse model of classic galactosemia. Mol Ther. 2020;28:304–12.
42. Drabavicius G, Daelemans D. Intermedilysin cytolytic activity depends on heparan sulfates and membrane composition. PLoS Genet. 2021;17: e1009387.
43. Sheen J. Master regulators in plant glucose signaling networks. J Plant Biol. 2014;57:67–79.
44. Damari-Weissler H, Kandel-Kfir M, Gidoni D, Mett A, Belausov E, Granot D. Evidence for intracellular spatial separation of hexokinases and fructokinases in tomato plants. Planta. 2006;224:1495–502.
45. Stryiński R, Mateos J, Carrera M, Jastrzębski JP, Bogacka I, Łopieńska-Biernat E. Tandem mass tagging (TMT) reveals tissue-specific proteome of L4 larvae of *Anisakis simplex* ss: Enzymes of energy and/or carbohydrate metabolism as potential drug targets in anisakiasis. Int J Mol Sci. 2022;23: 4336.
46. Negrete-Hurtado A, Overhoff M, Bera S, De Bruyckere E, Schätzmüller K, Kye MJ, et al. Autophagy lipidation machinery regulates axonal

microtubule dynamics but is dispensable for survival of mammalian neurons. Nat Commun. 2020;11:1535.
47. Qi H, Li J, Xia F-N, Chen J-Y, Lei X, Han M-Q, et al. Arabidopsis SINAT proteins control autophagy by mediating ubiquitylation and degradation of ATG13[OPEN]. Plant Cell. 2020;32:263–84.
48. Vicencio E, Cordero EM, Cortés BI, Palominos S, Parra P, Mella T, et al. *Aggregatibacter actinomycetemcomitans* induces autophagy in human junctional epithelium keratinocytes. Cells. 2020;9: 1221.
49. Zhang B, Shao L, Wang J, Zhang Y, Guo X, Peng Y, et al. Phosphorylation of ATG18a by BAK1 suppresses autophagy and attenuates plant resistance against necrotrophic pathogens. Autophagy. 2021;17:2093–110.
50. Lee J, Kim J, Lee J-H, Choi YM, Choi H, Cho H-D, et al. SIRT1 promotes host protective immunity against *Toxoplasma gondii* by controlling the FoxO-autophagy axis via the AMPK and PI3K/AKT signalling pathways. Int J Mol Sci. 2022;23: 13578.
51. Rockenfeller P, Koska M, Pietrocola F, Minois N, Knittelfelder O, Sica V, et al. Phosphatidylethanolamine positively regulates autophagy and longevity. Cell Death Differ. 2015;22:499–508.
52. Wilson-Zbinden C, dos Santos AX da S, Stoffel-Studer I, van der Vaart A, Hofmann K, Reggiori F, et al. Autophagy competes for a common phosphatidylethanolamine pool with major cellular PE-consuming pathways in saccharomyces cerevisiae. Genetics. 2015;199:475–85.
53. Patel S, Dinesh-Kumar SP. Arabidopsis ATG6 is required to limit the pathogen-associated cell death response. Autophagy. 2008;4:20–7.
54. Liu C, Liu M, Yang L, Zhang X. Influence of ripening stage and meteorological parameters on the accumulation pattern of polyphenols in green-gages (Prunus mume Sieb. Et Zucc) by widely targeted metabolomic. Curr Res Food Sci. 2022;5:1837–44.
55. Chung CZ, Jaramillo JE, Ellis MJ, Bour DYN, Seidl LE, Jo DHS, et al. RNA surveillance by uridylation-dependent RNA decay in *Schizosaccharomyces pombe*. Nucleic Acids Res. 2019;47:3045–57.
56. Humbert M, Seiler K, Mosimann S, Rentsch V, Sharma K, Pandey AV, et al. Reducing *FASN* expression sensitizes acute myeloid leukemia cells to differentiation therapy. Cell Death Differ. 2021;28:2465–81.
57. Jia X, Zhu Y, Hu Y, Zhang R, Cheng L, Zhu Z, et al. Integrated physiologic, proteomic, and metabolomic analyses of *Malus halliana* adaptation to saline–alkali stress. Hortic Res. 2019;6:91.
58. Naeem M, Zaman W, Saqib S, Shahzad A, Rahman SUR, Ahmad N. CRISPR/Cas-mediated genome editing for efficient tomato breeding: past achievements and future directions. South African J Botany. 2024;172:277–88.
59. Naeem M, Waseem M, Zhu Z, Zhang L. Downregulation of *SlGRAS15* manipulates plant architecture in tomato (*Solanum lycopersicum*). Dev Genes Evol. 2020;230:1–12.

Publisher's Note